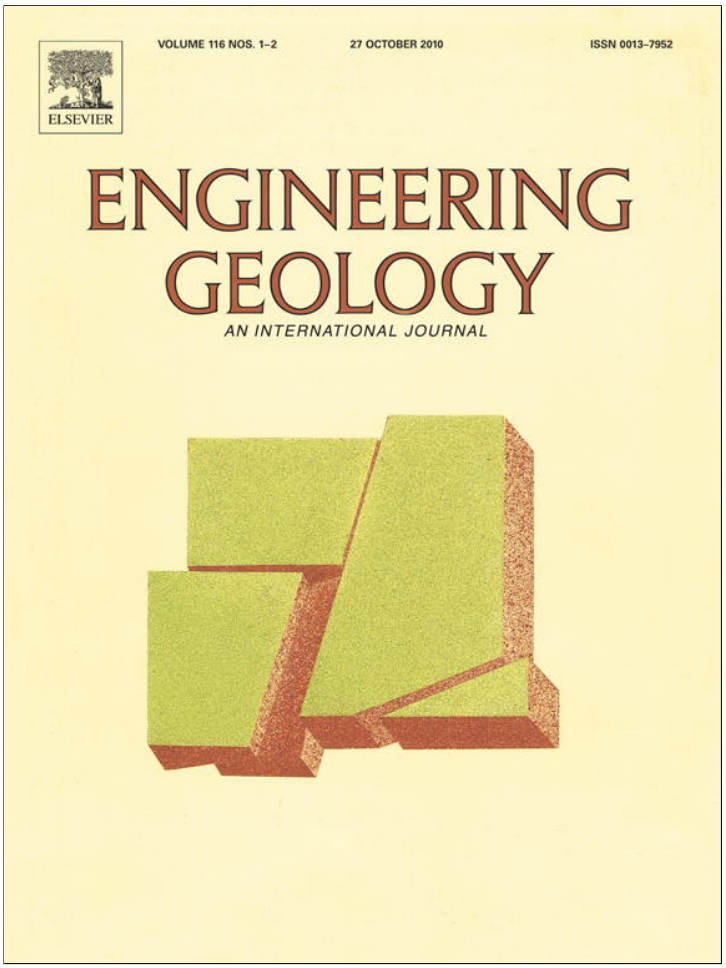

Engineering Geology 116 (2010) 73–85

Contents lists available at ScienceDirect

Engineering Geology

journal homepage: www.elsevier.com/locate/enggeo

Fluid transport properties and estimation of overpressure at the Lusi mud volcano, East Java Basin

Wataru Tanikawa [a,*], Masumi Sakaguchi [b], Handoko Teguh Wibowo [c], Toshihiko Shimamoto [d], Osamu Tadai [b]

[a] Kochi Institute for Core Sample Research, Japan Agency for Marine-Earth Science and Technology, Nankoku, Japan
[b] Marine Works Japan Ltd., Nankoku, Japan
[c] Sidoarjo Mudflow Mitigation Agency (SMMA), Surabaya, Indonesia
[d] Department of Earth and Planetary Systems Science, Graduate School of Science, Hiroshima University, Higashi-Hiroshima, Japan

ARTICLE INFO

Article history:
Received 10 September 2009
Received in revised form 9 July 2010
Accepted 19 July 2010
Available online 24 July 2010

Keywords:
Mud volcano
Lusi
Permeability
Sedimentary basin
Overpressure
Fluidization

ABSTRACT

Generation and maintenance of overpressure can prevent sediments from compaction and weaken sedimentary rocks in deep basins. Excess fluid pressure is one of the key factors to explain the disastrous mud eruption that took place in Sidoarjo, East Java, on 29 May 2006, though the mechanism by which it developed is not well known. We measured permeability and specific storage at a confining pressure of 100 MPa in outcrop samples from the East Java Basin. Both permeability and specific storage in our samples showed large stratigraphic variations. The mudstone of the Upper Kalibeng Formation that is thought to be the source of mud at Lusi had the lowest permeability of our samples at around 10^{-19}–10^{-20} m^2, and the permeability of the Upper Kujung Formation limestone was 10^{-16} m^2, which is two orders of magnitude larger than that of the Lower Kujung Formation limestone. In addition, the permeability and porosity of cemented sedimentary rocks showed low sensitivity to effective pressure. From numerical basin analysis of the Lusi site together with laboratory data, we evaluated the evolution of pore pressure and porosity histories and their present distributions. Our results show that high overpressure was generated below the mudstone of the Upper Kalibeng Formation and almost reached lithostatic levels. The modeled fluid pressure variation is consistent with the observed data. The long-lived overpressure at depth is mainly caused by the existence of thick low-permeability sediments and a high sedimentation rate. Undercompaction of the Upper Kalibeng Formation because of overpressurization may have caused the mud to lose strength and cause liquefaction (and hydrofracturing) as a result of small stress fluctuations induced by the Yogyakarta earthquake, which may have ended up causing the mud eruption.

1. Introduction

On 29 May 2006, an unexpected water and mud eruption took place in the Porong subdistrict of Sidoarjo, East Java (Fig. 1a and b). This mud volcano is commonly called Lusi (Lumpur "mud"-Sidoarjo), and the eruption occurred during drilling of the Banjar Panji-1 gas exploration well at a site only 150–200 m away from the point where the eruption started (Davies et al., 2007). After the start of the mud eruption, the rate of mud flow was from 5000 to 120,000 m^3/day for the first three months, and it still continues after three years. The strong flow has begun to cause subsidence, and a caldera has begun to form. On the basis of clay mineralogy, vitrinite reflectivity, and biostratigraphy, the erupted mud is derived from between 1615 and 1828 m depth in the Upper Kalibeng Formation (Mazzini et al., 2007). Geochemical analyses of gas and fluid at the eruption site suggest that the gas and water are sourced from both shallow and deep formations, and may come from as deep as the Kujung Formation.

Davies et al. (2007) suggest that the eruption of mud was triggered by the connection of strata at high fluid pressures to the surface via fractures created either by drilling or as a result of an earthquake (the Yogyakarta earthquake, 6.3 in magnitude, occurred on 27 May 2006). There is some doubt about the earthquake hypothesis as the earthquake occurred two days before the mud eruption and 280 km distant from the well (Davies et al., 2007). Davies et al. (2008) and Tingay et al. (2008) evaluated the possible pore pressure and stress changes triggered by the earthquake, but their estimated changes were only a few tens to hundreds of Pa, and are much smaller than the stress changes that can be caused by tides or variations of barometric pressure. The hypothesis that the eruption was induced by the earthquake is supported by the observation that the partial loss of drilling mud during drilling of the Banjar Panji-1 well occurred 10 min

* Corresponding author. Kochi Institute for Core Sample Research, Japan Agency for Marine-Earth Science and Technology, 200 Monobe-otsu, Nankoku 783-8502, Japan. Tel.: +81 88 878 2203; fax: +81 88 878 2192.
E-mail address: tanikawa@jamstec.go.jp (W. Tanikawa).

0013-7952/$ – see front matter © 2010 Elsevier B.V. All rights reserved.
doi:10.1016/j.enggeo.2010.07.008

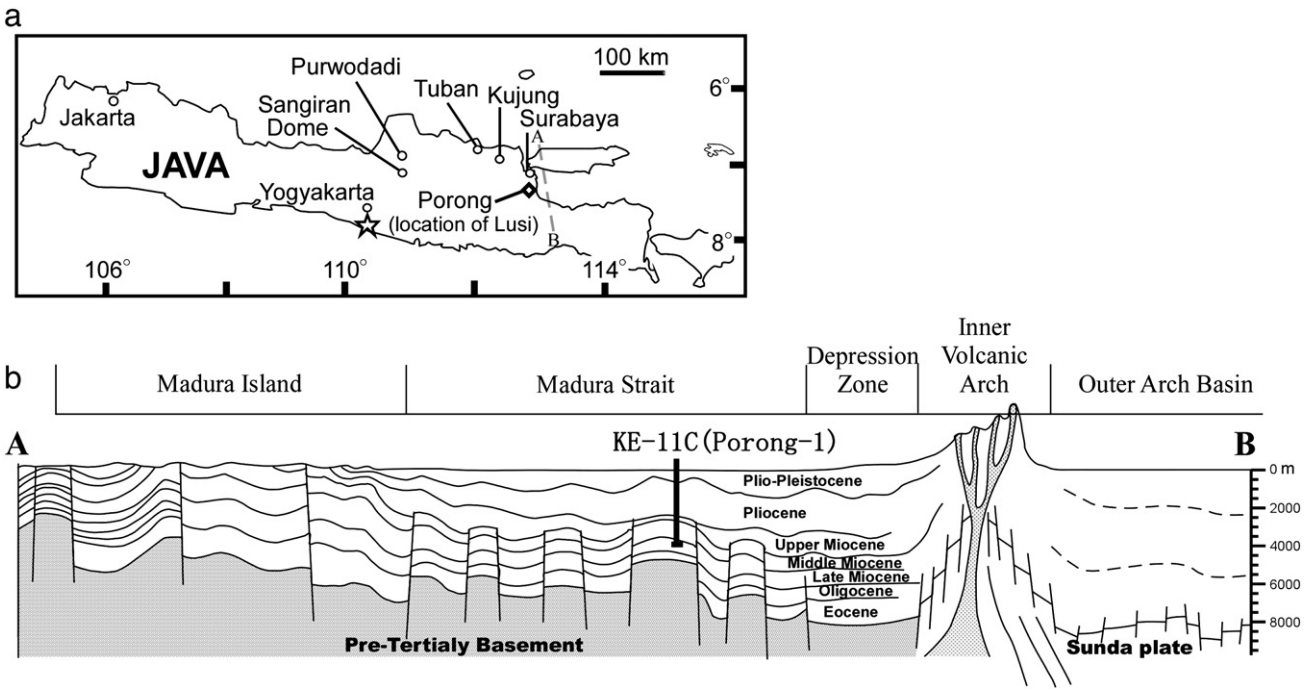

Fig. 1. (a) Map of Java Island showing the location of the Lusi mud volcano and the epicenter of the 2006 Yogyakarta earthquake (shown by a star). (b) North–south cross section across the Madura Strait (after Kusumastuti et al., 2002), and the location of KE-11C well which is near Porong well.

after the earthquake (Mazzini et al., 2007; Tingay et al., 2008). A different trigger mechanism was proposed by Davies et al. (2007, 2008), who suggested that gas exploration drilling triggered the mud volcano eruption. They assumed that there was sufficient influx of formation fluid into the borehole to cause hydraulic fracturing that may have propagated to the surface. Their assumption is based on a theoretical pressure analysis at 1091 m (the shallowest depth in the borehole without protective steel casing), which showed that pore pressure might have approached the formation pressure just before the eruption (Davies et al., 2008). They suggested that the removal of the drill bit between 27 and 28 May caused a kick event (influx of formation fluid and gas into the wellbore), and that fluid pressure generation after the well was shut in because of the kick was sufficient to cause hydrofracturing. The lack of casing below 1091 m increased the potential for hydraulic fracturing. However, Mazzini et al. (2007) argued that the formation of surface fractures observed at the well site during the second day of the mud eruption, with no fluid exiting from these fractures, was caused by shearing rather than by hydrofracturing.

Drilling records and sonic-log data from the Banjar Panji-1 well (Fig. 2) indicate the existence of overpressure in the Kalibeng Formation before the mud eruption. Excess fluid pressure reduces rock strength and, when it exceeds formation pressure, enhances fracturing. If the overpressure at depth was close to lithostatic pressure, even a small perturbation of pore pressure might have caused hydrofracturing. Overpressure caused by loading prevents consolidation of sediments. For high porosity sediments with less lithification, the resultant under-compaction enhances the mobility of sediments and causes fluidization. Such soft sediments at depth can become fluidized and sometimes form mud volcanoes. Mud volcanoes erupt water, fine sediment, fragments of country rock, and, sometimes, oil and natural gas. Lusi has all of these characteristics and is therefore considered to be a mud volcano. Mud volcanoes are most often found in areas where high sedimentation rates together with impermeable sediments lead to the development of high pore pressures (Kopf, 2002).

Several mechanisms have been proposed for the generation of overpressure in thick sedimentary basins (Osborn and Swarbrick, 1997; Wangen, 2001), and it is generally accepted that rapid sediment loading on low-permeability formations is an important factor (Bredehoeft and Hanshaw, 1968). Dehydration reactions, hydrocarbon generation, and the additional influx of water from depth are other possible mechanisms (e.g., Tanikawa et al., 2008). Permeability and specific storage are critical hydraulic properties that control the generation of overpressure and the distribution of fluid pressure at depth (Gibson, 1958; Bethke and Corbet, 1988).

However, fluid transport properties and the mechanism of generation of regional overpressure at Lusi and elsewhere in the East Java Basin are not well understood. Consequently, we investigated the mechanism by which overpressure was generated by using measured transport properties and a simplified one-dimensional basin model. We used outcrop samples from the East Java Basin to assess the fluid transport properties that are likely to exist at the Lusi drilling site.

2. Geological setting

The Lusi mud volcano erupted in the south of the East Java Basin, which is an inverted backarc basin. The structural history of the East Java Basin is divided into two phases: a Middle Eocene to Oligocene extensional phase, and a Neogene compressional or inversion phase. Grabens and half-graben structures were developed during the extensional phase, which was followed in the Neogene by compressional deformation with some wrenching. The most recent sedimentation in the East Java Basin occurred during the Late Pliocene to Holocene (3.6–0 Ma), during which time the southern part of the basin (Kendeng zone) was affected by north-verging thrusts and uplift. The uplift was accompanied by an influx of volcaniclastic rocks from the volcanic arc. From the Oligocene to the Holocene, the basin filled with shallow-marine carbonates and marine muds. The overpressuring was thought to be caused mainly by high sedimentation rates followed by rapid subsidence and maturation of organic materials (Willumsen and Schiller, 1994; Schiller et al., 1994), though detailed transport property data that are strongly connected to pore pressure generation were not reported.

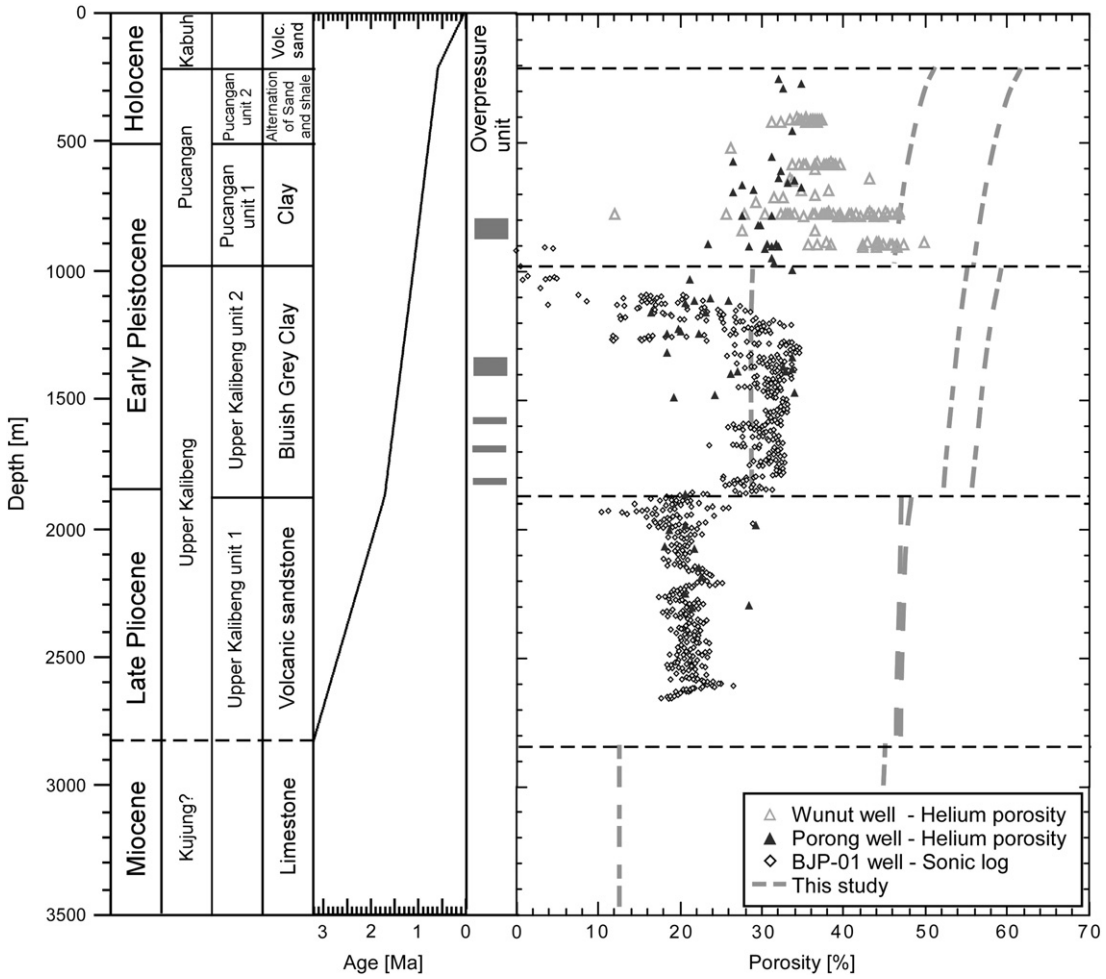

Fig. 2. Stratigraphic column, sediment accumulation history, possible overpressured zones, and porosity–depth plot for the Banjar Panji-1 well. The age vs. depth plot (used for our numerical basin model) was modified from unpublished data provided by Lapindo Brantas Inc. Porosity data was derived from sonic-log data from the Banjar Panji-1 well (Lapindo Brantas Inc., personal communication) and from core samples from the Wunut well (Huffco Brantas Inc., personal communication) and the Porong well (Lapindo Brantas Inc., personal communication). A porosity curve from sonic-log data in the Banjar Panji-1 well was computed by using the acoustic formation factor equation of Raiga-Clemenceau et al. (1988), assuming the acoustic formation factor = 2.19.

There are several mud volcanoes in East Java; of these, the Kalang Anyar mud volcano, 30 km to the northeast, is the nearest to Lusi. A number of the mud volcanoes are in the vicinity of the northeast–southwest trending Watukosek Fault, the escarpment of which extends northeast toward Lusi. Today, some parts of Sidoarjo are subsiding and others are being uplifted, suggesting that the Watukosek Fault was reactivated during the 2006 Yogyakarta earthquake and eruption of the Lusi mud volcano (Mazzini et al., 2007).

The stratigraphy at Lusi (Fig. 2) consists of (1) alluvial sediments, (2) Pleistocene alternating sandstone and shale of the Pucangan Formation (to about 500 m depth), (3) Pleistocene clay of the Pucangan Formation (to about 1000 m depth), (4) Pleistocene bluish gray clay of the Upper Kalibeng Formation (to 1871 m depth), and (5) Late Pliocene volcaniclastic sand of at least 962 m thickness. The stratigraphy below the Late Pliocene sand is not well known; however, when the Banjar Panji-1 gas well reached 2834 m depth, mud circulation in the well was lost, which suggests that drilling mud was escaping from the borehole into neighboring porous rocks. Davies et al. (2007) suggested that these porous rocks were Kujung Formation limestone and that this formation is the source of the fluids erupting at Lusi. Seismic correlations from the Porong-1 well, 6.5 km to the northeast of Lusi, also indicate that the rocks underlying the Late Pliocene volcaniclastic sands are from the Kujung Formation.

3. Fluid pressures in the Banjar Panji-1 gas exploration well

A leak-off test was carried out at 1091 m depth in the Banjar Panji-1 well, which corresponds to the depth of the deepest casing shoe. From the leak-off test data, Davies et al. (2008) calculated the leak-off pressure (formation pressure) at that depth to be in the range 19.6–21.03 MPa. They also estimated fluid pressure at the same depth when the well was shut in. From mud weight data and pore pressures, they estimated a fluid pressure of 21.29 MPa, which indicates that fluid pressure at 1091 m depth was elevated higher than the formation pressure just before the mud eruption. Stratigraphic variations of porosity at the Lusi drilling site evaluated from sonic-log data (Fig. 2, Lapindo Brantas Inc., personal communication) show a porosity transition between the Pucangan Formation and the Upper Kalibeng Formation. The transition zone is observed in the Upper Kalibeng Formation at 1850 m depth as well. This implies that the Upper Kalibeng Formation at a shallower horizon is overpressured. Davies et al. (2007, 2008) proposed that the limestone of the Kujung Formation below 2800 m depth is overpressured and that this provided the trigger for the tremendous Lusi mud flow.

4. Experimental procedure

We used outcrop samples from the East Java Basin for our laboratory tests. As it was difficult to find fresh outcrops of all of the

stratigraphic units that correlate to the sequence at Lusi, we collected samples to cover the stratigraphic range from the Lower Kujung Formation limestone to the Pucangan Formation sandstone and siltstone (Table 1).

We collected block samples from which we cut cylindrical cores (20 mm diameter, 10 to 30 mm length), which we dried in an oven at 80 °C for one week to eliminate water from the pore spaces. After drying, we measured matrix volumes with a commercial pycnometer (Penta pycnometer, Quantachrome Instruments, Florida, USA). We determined porosity and grain density at atmospheric pressure from the measured matrix volume. Grain densities (= matrix weight/matrix volume) ranged from 2.4 to more than 2.8 g/cm^3 (Table 1). Grain matrix volume data were used for porosity measurements under high confining pressure. To evaluate mineral composition of the samples, we used X-ray diffraction analysis of powdered subsamples.

The cylindrical samples were imaged using a micro-focus X-ray CT system (HMX225-ACTIS+3, Tesco Co. Ltd., Tokyo, Japan). The X-ray focus was 5 μm, the X-ray tube voltage was 120 kV, and the tube current was 30 mA. The magnification factor (ratio of detector–source distance to sample–source distance) was 2.0. The pixel size of the 2-D detector (the resolution of the image) was 0.106×0.106 mm.

We measured permeability and porosity at room temperature under uniform (isostatic) confining pressure in a high-oil-pressure apparatus. Permeability was measured by the steady-state flow method (e.g., Bernabe, 1987) and the pulse-decay method (Zoback and Byerlee, 1975) with distilled water used as the pore fluid. Gas permeability was measured by the steady-state gas flow method (Wu et al., 1998; Tanikawa and Shimamoto, 2009) with nitrogen gas used as the pore fluid. In the steady-state flow method, a constant pressure gradient is applied through the sample, and the permeability is determined according to the following equation:

$$Q = \frac{k_w A}{\eta L}\left(P_{up} - P_{down}\right) \tag{1}$$

where Q is the volume of fluid measured per unit time, k_w is water permeability, A is the cross-sectional area of the sample, η is the dynamic viscosity of the fluid, L is sample length, and P_{up} and P_{down} are pore pressures at the upstream and downstream ends of the specimen. When a condensable gas is used as the pore fluid, the density of the pore fluid differs within the specimen. In this case, the gas permeability (k_{gas}) is expressed (Wu et al., 1998)

$$Q = \frac{A k_{gas}}{2\eta L}\left(\frac{P_{up}^2 - P_{down}^2}{P_{down}}\right) \tag{2}$$

For the steady-state flow measurements of both water and gas, we kept P_{up} constant by using a pressure regulator (0.10 to 1.6 MPa). We monitored the rate of water outflows from the lower end of the samples with a commercial digital balance to monitor water flows, and we used gas flow meters (ADM2000, Agilent Technology, California, U.S.A.) to monitor gas flows. We assumed a constant value of 0.1 MPa for P_{down} as the water and gas flowing out of the lower end of the specimen was released to atmospheric pressure (0.1 MPa). Porosity changes in response to confining pressure changes were determined by the gas-expansion method (Scheidegger, 1974; Wibberley and Shimamoto, 2005). When fluid compression is considered, and assuming that the rock grains are much less compressible than pore spaces (e.g., compressibility of mica is 1.2×10^{-11} Pa^{-1}, independent of pressure (Birch, 1966)), specific storage (Ss) was calculated by using porosity data in the following equation:

$$Ss = \beta_\Phi + \Phi\beta_f, \tag{3}$$

where β_Φ is drained compressibility, β_f is compressibility of pore fluid, and Φ is porosity. The drained pore compressibility was expressed as

$$\beta_\Phi = -\frac{1}{V_p}\frac{\partial V_p}{\partial Pc}\bigg|_{P=0} = -\frac{1}{1-\Phi}\frac{\partial \Phi}{\partial Pc}\bigg|_{P=0}, \tag{4}$$

where V_p is pore volume, Pc is confining pressure, and P is pore pressure. During our porosity measurements, the pore pressure change is extremely small compared with the confining pressure change (in our test, the pore pressure change was less than 0.01 MPa for a step change in confining pressure of 10 MPa).Therefore we assumed that the condition of the sample was “drained” when pore pressure was constant. Above these assumptions, to determine specific storage, we calculated the drained pore compressibility from Eq. (4) using the results of the porosity measurements (Wibberley and Shimamoto, 2005).

5. Results

5.1. Mineralogy and microstructure

The mineral compositions of sedimentary rocks used for the laboratory experiments are shown in Table 2. Hot mud slurry from Lusi contains quartz, calcite, anorthite, smectite, illite, kaolinite, chlorite, and halite, which, with the exception of chlorite and halite, is a similar mineral assemblage to that of a brownish shale in the Kalibeng Formation. The halite might come from seawater trapped during deposition of the Kalibeng Formation. The mineral composition that we determined for Lusi mud is consistent with a previous report by Plumlee et al. (2008), although they also identified pyrite, which we did not. The so-called limestone of the Upper Kujung Formation is composed mainly of grains of dolomite cemented and veined with calcite. Several sedimentary rocks in the Lusi sequence are cemented by carbonate. Some shales in the Kalibeng Formation are cemented by dolomite, though some are not. Upper and Lower Kujung Formation limestones are cemented with calcite. The average grain size of the Upper Kujung Formation is much larger (0.5 mm in two dimensions) than that of the Lower Kujung Formation (Figs. 3 and 4).

CT values reflect grain density and chemical composition. High CT values indicate high density and high atomic weight (Hirono et al., 2003). Cemented shale (Kalibeng Formation) and cemented

Table 1
Physical properties and location of outcrop samples used in laboratory tests.

	Matrix density [g/cm^3]	Porosity [%] at 0.1 MPa	Permeability [m^2] at 10 MPa	Sampling location	Representative unit for BJP-1well
Pucangan Fm — pebble	2.52	48.5	1.6×10^{-14}	Desa Kepuh Klagen, Gresik	Pukangan Fm unit 2
Pucangan Fm — siltstone	2.41–2.49	52.4–54.8	2.6×10^{-18}	Desa Kepuh Klagen, Gresik	Pukangan Fm unit 1
Kalibeng Fm — siltstone	2.54–2.66	56–58.5	$2.6–7.1\times10^{-20}$	Desa Kepuh Klagen, Gresik	Upper Kalibeng Fm unit 2
Kalibeng Fm — cemented siltstone	2.76–2.79	26.5–29	4×10^{-18}	Desa Kepuh Klagen, Gresik	Upper Kalibeng Fm unit 2
Kalibeng Fm — sandstone	2.77–2.97	45–60	2×10^{-13}–7.4×10^{-14}	Desa Kepuh Klagen, Gresik	Upper Kalibeng Fm unit 1
Upper Kujung Fm	2.83	54.2	$1.6–1.8\times10^{-14}$	Desa Kujung, Tuban	Kujung Fm
Lower Kujung Fm	2.76–2.8	12–30	1.6×10^{-16}–1.2×10^{-17}	Desa Kujung, Tuban	Kujung Fm

Table 2
Mineral composition of outcrop samples measured by XRD analyses. ○, clearly observed; ▲, rarely observed.

	Quartz	Dolomite	Calcite	Albite	Anorthite	Smectite	Illite	Kaolinite	Chlorite	Halite
Pucangan Fm	○			○	○	○		○		
Kalibeng Fm siltstone	○		○	▲	▲	○	○	○		
Kalibeng Fm-cemented	○	○			▲	○	○	○		
Kalibeng Fm-sandstone	○		○	○	○	○				
Upper Kujung Fm		○								
Lower Kujung Fm		○	○							
Muddy water in LUSI	○		○		▲	○	○	○	○	○

limestone (Lower Kujung Formation) showed relatively high CT values in the CT scan images (Fig. 3). Some fossils in the porous limestone of the Upper Kujung Formation have retained their original shapes (Fig. 4c). The CT images do not clearly show pore space and shape in most of the Lower Kujung Formation sample, but isolated pores of more than 0.5 mm in diameter are in evidence. The average pore size in the Lower Kujung Formation is much smaller than that of the Upper Kujung Formation.

5.2. Transport properties

Cyclic effective pressure tests were performed on all specimens. Confining pressure was first increased from 0 to 100 MPa, and then decreased to 0 MPa. The maximum confining pressure (100 MPa) in the laboratory tests is equivalent to 6.8 km depth at hydrostatic condition, which covers the thickness of the Java basin at Lusi. We measured permeability and porosity at various confining pressures. Water permeability in all specimens decreased with increasing effective pressure, and the sensitivity to pressure of permeability decreased as effective pressure increased (Fig. 5a). The highest permeabilities were measured in Upper Kujung Formation samples, ranging from 4×10^{-14} to 1×10^{-16} m^2. The lowest permeabilities were measured in the Kalibeng Formation mudstone, ranging from 2×10^{-19} to 4×10^{-21} m^2. Permeabilities of Upper Kujung Formation samples were much higher than those of Lower Kujung Formation samples, and were similar to the permeabilities of conglomerates and sandstones elsewhere in the sequence. The sensitivity of permeability to effective pressure varied among specimens. The permeability of cemented Kalibeng Formation samples and Lower Kujung Formation samples decreased by less than one order of magnitude as effective pressure increased to 100 MPa. All of the other samples showed much more pressure dependence; permeability decreased by two to more

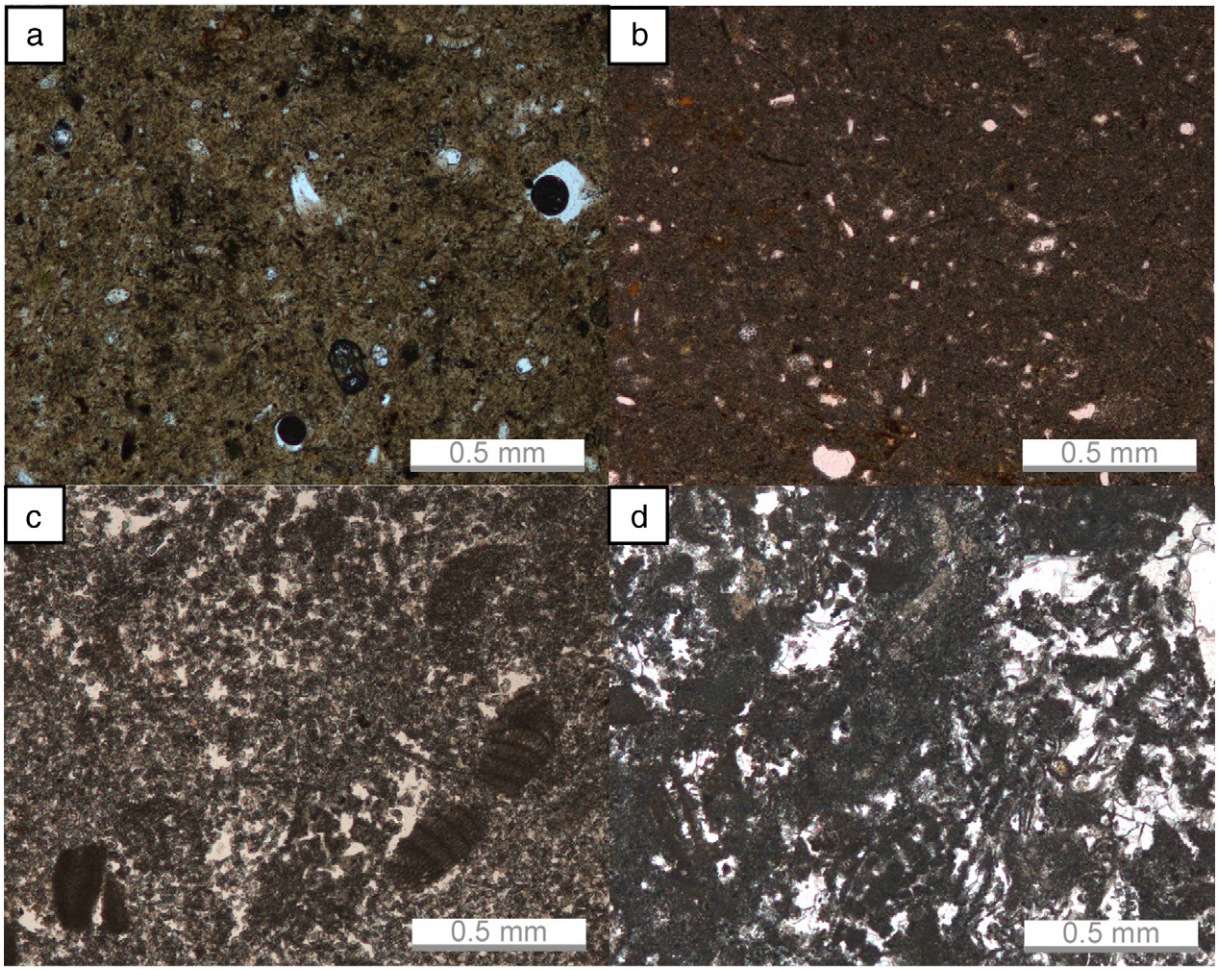

Fig. 3. Microphotographs of samples used for permeability measurement. (a) Kalibeng Formation brownish siltstone, (b) Kalibeng Formation siltstone with cementation, (c) Upper Kujung Formation porous limestone, (d) Lower Kujung Formation limestone.

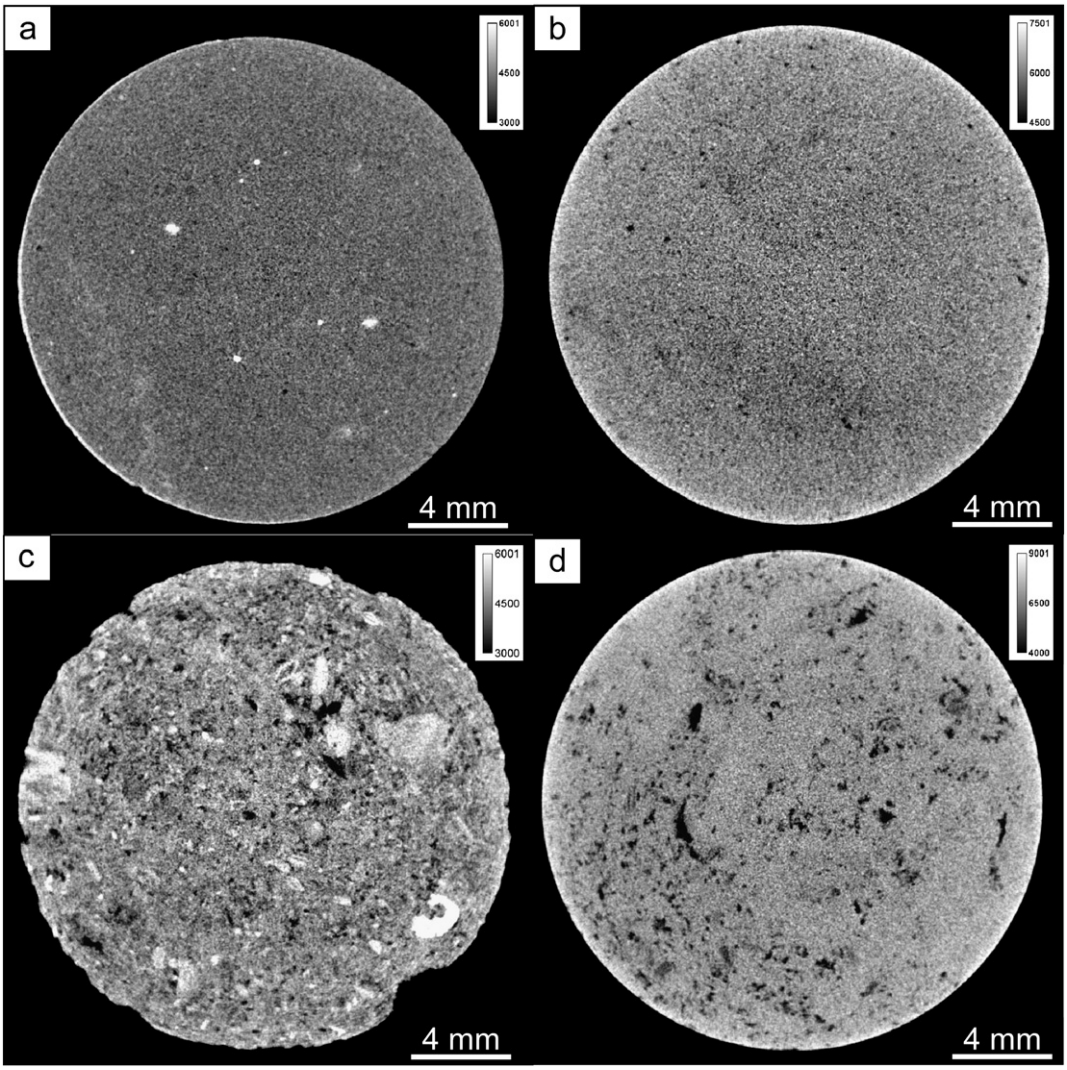

Fig. 4. CT image of samples used for permeability measurement. Relative CT values are indicated by gray-scale bars beside each image. (a) Kalibeng Formation brownish siltstone, (b) Kalibeng Formation siltstone with cementation, (c) Upper Kujung Formation porous limestone, (d) Lower Kujung Formation limestone.

than three orders of magnitude as effective pressure was increased to 100 MPa. The cyclic effective pressure test of Pucangan Formation sandstone showed a small water permeability increase during depressurization, and the permeability did not recover its initial value, even at the lowest effective pressure.

Gas permeability was higher than water permeability for all samples, although the sensitivities to effective pressure of gas and water permeabilities were similar (Fig. 5b). Gas permeability of Upper Kujung Formation samples ranged from 1×10^{-13} to 4×10^{-15} m^2, which is greater by a factor of about five than the water permeability of the same formation. The largest difference between water and gas permeabilities was observed in Kalibeng Formation samples, where the water permeability was two orders of magnitude lower than the gas permeability. Lower Kujung Formation samples showed very small differences between water and gas permeabilities. The gas permeability of the cemented samples of Kalibeng Formation and Lower Kujung Formation samples decreased little as effective pressure increased to 100 MPa.

Porosity in all specimens decreased as effective pressure increased, but the initial porosity and rate of porosity reduction varied among samples (Fig. 6a). The rate of porosity reduction declined as effective pressure increased, which is a similar trend to that observed for permeability. Both Kalibeng Formation cemented siltstone and Lower Kujung Formation limestone showed small reductions in porosity as effective pressure increased, though other porous sedimentary rocks showed sharp reductions in porosity to as low as 10% of initial porosity at maximum effective pressure.

The porous and compressible rock samples showed high specific storage (Fig. 6b). Initially, specific storages were around 10^{-8} Pa^{-1}; they then decreased almost linearly with increasing effective pressure. Specific storage decreased by one order of magnitude to 10^{-9} Pa^{-1} at maximum effective pressure. In contrast, incompressible Kalibeng Formation cemented siltstone and Lower Kujung Formation limestone showed low specific storages and low sensitivity of specific storage to pressure. For these samples, specific storage decreased by less than a factor of two at maximum effective pressure.

6. Numerical analysis

6.1. Modeling parameters

To analyze the history of overpressure generation in the Lusi area on a geological time scale, we used a one-dimensional basin model initially designed by Bredehoeft and Hanshaw (1968) and further developed by later researchers (e.g., Bethke and Corbet, 1988;

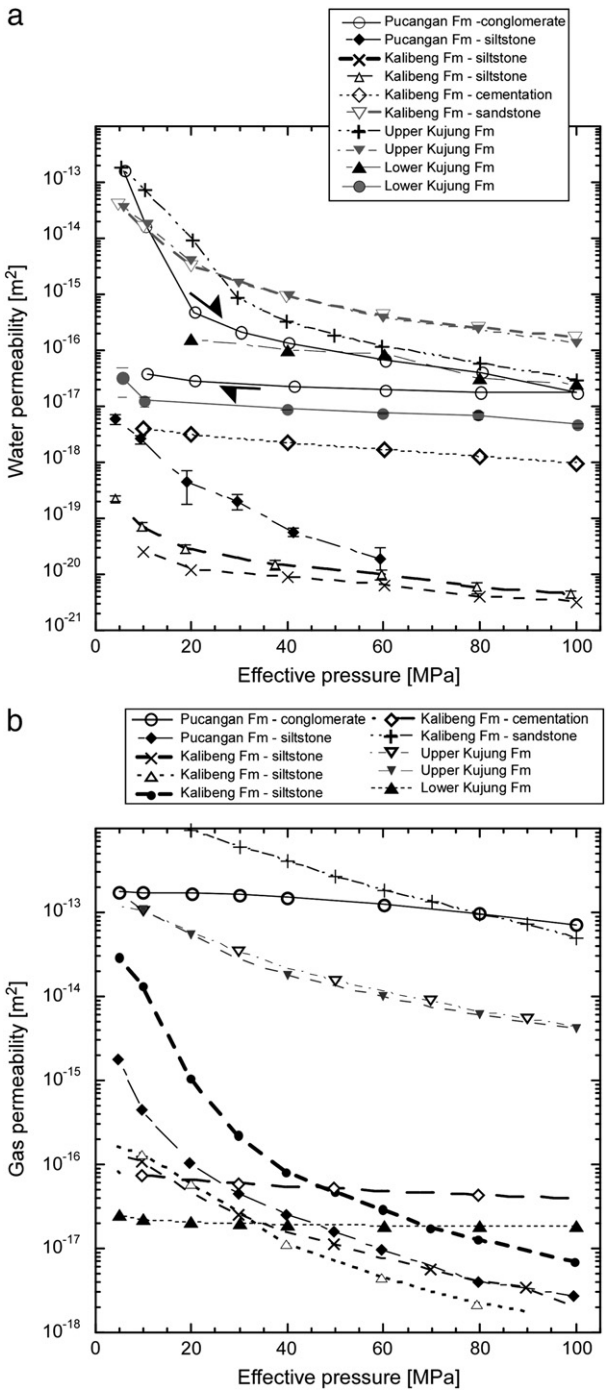

Fig. 5. (a) Water permeability and (b) gas permeability of sedimentary rocks from the East Java Basin as a function of effective pressure. A small decrease of water permeability is shown in conglomerate from the Pucangan Formation during depressurization. Gas permeability was measured by using nitrogen gas at low pressures in the range from 0.05 to 1.5 MPa.

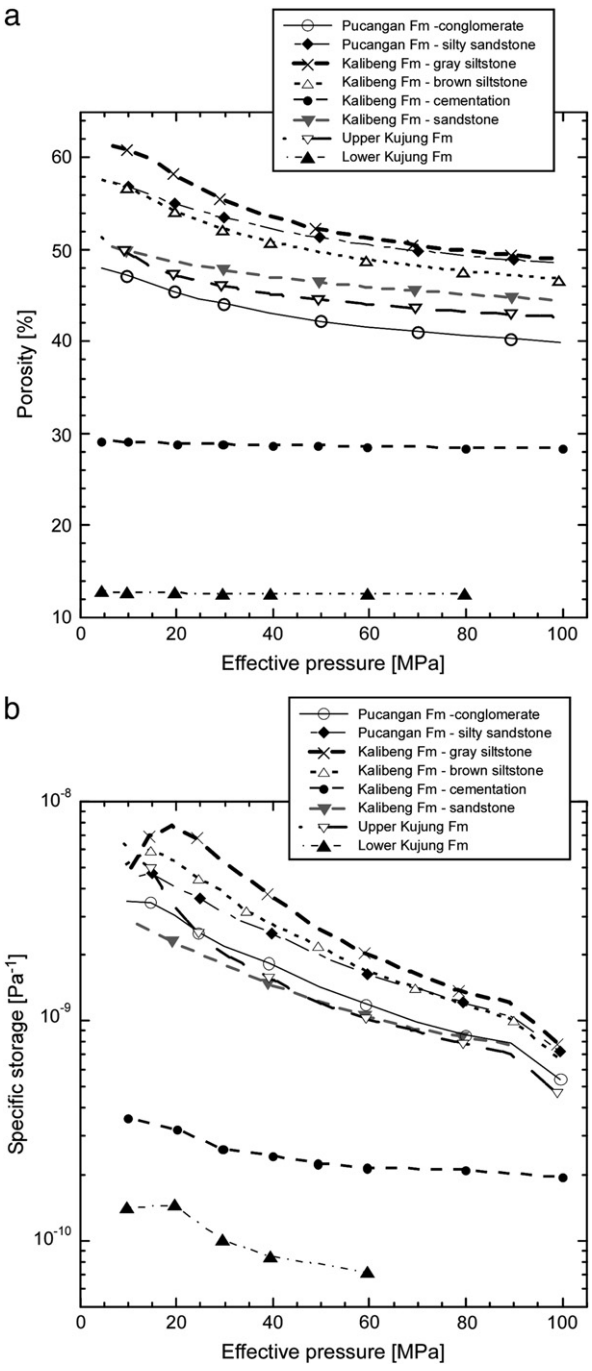

Fig. 6. (a) Porosity and (b) specific storage of sedimentary rocks from the East Java Basin as a function of effective pressure. Specific storage was estimated from porosity data.

Wangen, 2001). This model satisfies our interest to know the influence of sedimentation history and stratigraphic variation of transport properties on overpressure generation. Even though the tectonic deformation history of the East Java basin from Miocene to the present is not well known, the present structure (Fig. 1b) indicates that the tectonic structure near Lusi site (Madura strait) is not deformed much and faults are rarely developed above Miocene formation. Therefore one-dimensional model can be applied to the Lusi region in basin analysis. In our modeling, we assumed water to be the only flowing medium; gas and oil were not considered. Pore pressure in the model was assumed to be generated in thick sediments by rapid vertical sediment loading and the thermal expansion of water in a state of constant heat influx. Our laboratory results show permeability of Kujung formation ranges 10^{-15} m^2 (permeable) to 10^{-18} m^2 (relatively impermeable), therefore, in this study, we considered two extreme cases. These were (a) that the Kujung Formation is permeable and (b) that the Kujung Formation is impermeable. We assumed that the Kujung Formation is a basement and that the boundary is located between the Kujung and Kalibeng Formations. For the case of impermeable Kujung Formation, we assumed that sediment accumulates on an impermeable basement (flux $q = 0$ m/s or permeability $k_w = 0$ m^2 for the entire period of sedimentation). For the case of permeable Kujung Formation, pore

pressure at the boundary was assumed to be always hydrostatic, so overpressure was always 0 MPa. The model equation can be written as follows (Bethke and Corbet, 1988; Luo and Vasseur, 1992):

$$\frac{\Delta P}{dt} = \frac{1}{Ss}\frac{\partial}{\partial z}\left(\frac{k_w}{\eta}\frac{\partial}{\partial z}P\right) + \frac{\beta_\Phi}{Ss}\frac{\Delta Pc}{dt} + \frac{1}{Ss}\left(\frac{\Phi\alpha_f \Delta T}{dt}\right), \quad (5)$$

where α_f is the thermal expansibility of the fluid, T is temperature, and the thermal expansibility of the grain matrix is assumed to be zero. Eq. (5) is based on Darcy's law, the law of mass conservation for both the fluid and the grain matrix, and Terzaghi's effective stress law. The second and third terms on the right-hand side of Eq. (5) are the terms that relate to the generation of pore pressure. $\Delta Pc/dt$ is equivalent to the burial rate, and $\Delta T/dt$ is related to both the geothermal gradient and the burial rate. The values of permeability and specific storage in Eq. (5) vary with depth and according to geological formation, as we showed in our laboratory tests. Because the samples we used for our laboratory tests were from an outcrop, not from the Banjar Panji-1 well (i.e., their depths of burial were not representative of the rocks encountered in the well), we had to assume that they were representative of the lithology and physical properties of the formations encountered in the Banjar Panji-1 well (Table 3). In other words, we assumed that the permeability of our outcrop sample of shale from the Upper Kalibeng Formation was the same as that in the Upper Kalibeng Formation unit 2 encountered in the well (Fig. 2; 980 to 1870 m depth). Based on the labolatory results, the stratigraphic variations of water and gas permeabilities and specific storage under hydrostatic conditions are described in Fig. 7, and they are also described as a function of effective pressure (Table 4). The data that we used to represent the relationship between water permeability and effective pressure for our numerical modeling are listed in Table 4; most of these are power law functions. Porosity data as a function of effective pressure used to numerical modeling, which were used to estimate the pore compressibility and specific storage from Eq. (4), are also listed in Table 4. These curves are described logarithmic function to effective pressure. From the well logging data in Fig. 2, the porosity–depth relationship at hydrostatic pressure (the normal consolidation curve) in the Banjar Panji-1 well can be also described as follows (Athy, 1930):

$$\Phi = \Phi_0 \exp(-\alpha \cdot Pe) \quad (6)$$

Here, Φ_0 is the initial porosity at surface (depth = 0 m), Pe is effective pressure, and α is a consolidation factor. $\Phi_0 = 60$ % was assumed from the reference of the other oil field (Magara, 1968). By fitting the Eq. (6) to the logging data, we assumed α was 5×10^{-8}. The specific storage–depth relationship is evaluated from the Eqs. (4) and (6) as well, and we found that the measured specific storage profiles using outcropping samples were similar to those predicted by Eq. (6) (Fig. 7). However, specific storage curves for Kalibeng Formation cemented siltstone and Lower Kujung Formation limestone determined by laboratory tests showed large deviation from the curve estimated from Eq. (6). Because we observed during our laboratory tests that the permeability of samples from the Upper Kalibeng Formation siltstone varied by more than one order of magnitude, we used three permeability curves for modeling the Upper Kalibeng Formation unit 1 to ensure that this range was covered (Table 4). We used different specific storage curve in the Upper Kalibeng Formation unit 1for different permeability curve as well.

Table 3
Physical properties used for numerical modeling.

Symbol	Value	Units	Comment and Reference
β_f	4.4×10^{-10}	Pa^{-1}	Compressibility of fluid (Luo and Vasseur, 1992) in Eq. (3)
α_f	5×10−4	$°C^{-1}$	Coefficient of thermal expansibility of fluid in Eq. (4) (Luo and Vasseur 1992)
ρs	2500	kg m^{-3}	Bulk density of sediments
ρw	1000	kg m^{-3}	Bulk density of water in Eq. (5)
$\partial T/\partial z$	42	°C km^{-1}	Geothermal gradient at Lusi site (Lapindo Brantas Inc., personal communication)
$\Phi 0$	0.6		Initial porosity in Eq. (6) used for porosity profile in Fig. 8b
α	5×10^{-8}	Pa^{-1}	Consolidation factor in Eq. (6) used for porosity profile in Fig. 8b
η	$2.414\times10^{-5}\times 10^{247.8/(T+133)}$	Pa s	Viscosity of water (Fontaine et al., 2001), T: temperature (K)

The model calculation starts with deposition of the Upper Kalibeng Formation in the Early Pliocene (3.2 Ma), and the sediment deposition continues through to the present. A total sedimentary sequence becomes 2820 m thickness. The history of sedimentation in the East Java Basin used for our modeling is that shown by the formation thickness and age relationships in the left-hand column of Fig. 2.

6.2. Modeling results

The present-day pore pressure distribution predicted by the model shows that pore fluid pressure is hydrostatic at shallow depths, and that overpressure is generated from the top of the Upper Kalibeng Formation mudstone (Fig. 8a). When the Kujung Formation is assumed to be permeable, overpressure is generated only within the low-permeability Upper Kalibeng 2 Formation. When the Kujung Formation is assumed to be impermeable, overpressure gradually increases with depth and its gradient becomes almost constant below 2000 m, and pore pressure approaches 50 MPa at depth. The predicted fluid pressure increases as permeability in Upper Kalibeng Formation unit 2 decreases. The predicted fluid pressure approaches lithostatic pressure at the depth of the Upper Kalibeng Formation unit 1 when the lowest permeability in Upper Kalibeng Formation unit 2 (A in Table 4) is assumed (around 10^{-20} m^2). On the other hand, little excess fluid pressure was modeled when the highest permeability in this formation (C in Table 4) was assumed (3×10^{-18} m^2). The present-day porosity distribution was also predicted by using modeled present-day fluid pressure distribution and the normal consolidation curve of Eq. (6) at Lusi site. Because the porosity–depth curve is related to the fluid pressure distribution, porosity increases within the overpressured layer (Fig. 8b). The trend of the predicted porosity distribution based on the consolidation curve from the logging data shows that porosity increases rapidly below Upper Kalibeng unit 2, and porosity approaches at its peak in the middle of Upper Kalibeng unit 2. This trend is not much different from both sonic-log and core sample data (Lapindo Brantas Inc., personal communication), and the logging data lies between the impermeable and permeable extremes we considered (Fig. 8c).

The predicted pore pressure distribution shows a similar trend to the maximum pore pressures that were estimated from drilling reports and leak-off tests (Fig. 9, Davies et al., 2007, 2008; Mazzini et al., 2007). When a permeability curve of B in Table 4 was used for the permeability of the Upper Kujung Formation unit 2, the pore pressure variations recorded at the well for shallow horizons were better reproduced compared to those in other permeability models in Table 4. On the other hand, modeled pressure curves that assumed hydrostatic pressure at the bottom boundary were very different from in situ pore pressure data.

The fluid pressure history in the basin model (Fig. 10) shows that overpressure was generated at 1.6 Ma, when the rate of deposition of the Upper Kalibeng Formation unit 1 increased to about 1.5 km/Myr. Maximum overpressure was reached at 0.56 Ma, when the sedimentation rate decreased abruptly to about 0.4 km/Myr. For the impermeable boundary condition, the overpressure generation history at the bottom was about the same as that at the lowermost

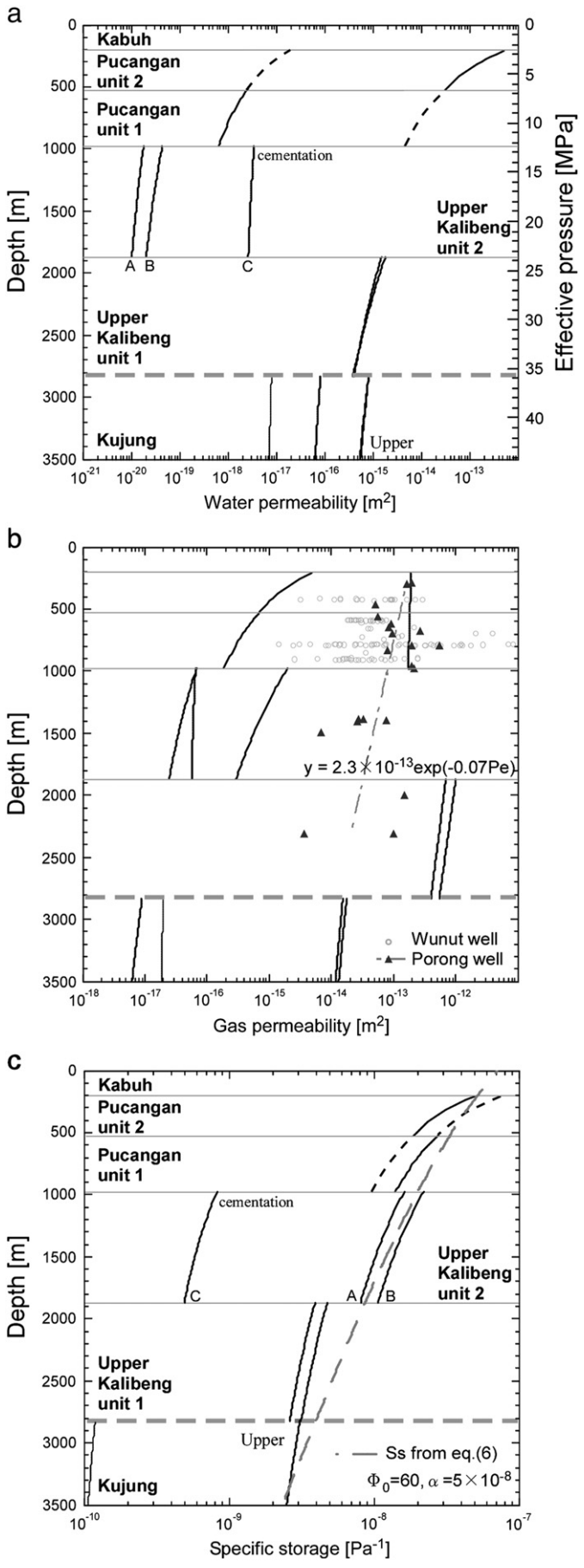

Table 4
Transport properties used for numerical modeling. *Pe*, effective pressure (MPa).

Formation	Depth (m)	Permeability (m^2)	Porosity (%)
Kabuh Fm	0–210	$1.8\times10^{-11}\ Pe^{(-3.1)}$	$54.9-7.4\log(Pe)$
Pucangan Fm unit 2	210–530	$1.8\times1^{0-11}\ Pe^{(-3.1)}$	$54.9-7.4\log(Pe)$
Pucangan Fm unit 1	530–980	$2.2\times10-^{16}\ Pe^{(-2.2)}$	$66.2-8.8\log(Pe)$
U Kalibeng Fm unit 2-A	980–1870	$1.8\times10^{-19}\ Pe^{(-0.85)}$	$67.3-10.4\log(Pe)$
U Kalibeng Fm unit 2-B	980–1870	$1.1\times10^{-18}\ Pe^{(-1.2)}$	$74.1-12.8\log(Pe)$
U Kalibeng Fm unit 2-C	980–1870	3.0×10^{-18}	$29.8-0.72\log(Pe)$
U Kalibeng Fm unit 1	1870–2830	$5.3\times10^{-11}\ Pe^{(-3.2)}$	$55.4-5.4\log(Pe)$

1000 m of the well (Fig. 10a). For the assumption of a permeable boundary condition, several abrupt changes in overpressure were modeled at 0.56 Ma (Fig. 10b).

7. Discussion

Our results show that high fluid pressure that is greater than hydrostatic pressure might have been generated within the Upper Kalibeng Formation of the Banjar Panji-1 borehole long before the Lusi mud eruptions. This is consistent with previous data measured in situ in the Banjar Panji-1 borehole. Our results indicate that the generation and maintenance of excess fluid pressure is attributable mainly to the very low permeability (less than 10^{-20} m^2) of sediments of the Upper Kalibeng Formation, which is similar to that of the Pierre Shale (Wu et al., 1997) and the Westerly Granite (Morrow et al., 1986). The rapid sediment loading (1500 m/Myr) during the Early Pleistocene is another important factor that contributed to overpressure at Lusi. The excess fluid pressure was generated mostly during periods of high sedimentation rate.

The generation of overpressure prevents the consolidation of sedimentary layers and sediment grains thus remain undeformed. Our modeled curve of porosity variation with depth shows a high porosity zone in the Upper Kalibeng Formation mudstone. That curve is consistent with porosity data estimated from the sonic-log data. However, our predicted curves do not reproduce the sonic-log porosity curve for deeper horizons. This indicates that the real boundary condition at 2830 m depth might be more complicated than either of our simple assumptions (permeable or impermeable); that is, at that depth the permeability of the rocks varies spatially between the two extremes we modeled, and that the fluid pressure at the boundary changes temporally because of variations in the influx of fluids from below. The relationship between porosity and gas permeability in Lusi (Fig. 11) shows that the general trend in the overpressured formation is deviated from the other samples, indicating the influence of overpressuring that prevent the consolidation of sediments.

7.1. Possible triggers for the Lusi eruption

The long-lived overpressure that was observed in the Upper Kujung Formation in the Banjar Panji-1 borehole developed during the evolution of the East Java Basin and might have contributed to the Lusi eruption. Various strength weakening mechanisms in solid particles filled with water are introduced in previous studies (e.g. Pudasaini and Hutter, 2007). The two processes that are the main cause of mobilization of mud sediments to form a viscous fluid are (1) liquefaction, and (2)

Fig. 7. Stratigraphic variation of (a) water permeability, (b) gas permeability and (c) specific storage at hydrostatic condition estimated from laboratory data. The variations of water permeability and specific storage with depth shown here were used for our numerical basin modeling. The curve of best fit for gas permeability from Wunut well and Porong well data (Huffco Brantas Inc., personal communication, and Lapindo Brantas Inc., personal communication, respectively) is shown as a dashed red curve. The specific storage profiles are also estimated from Eq. (6) using Wunut and Porong well porosity data. Three permeability and specific curves in Upper Kalibeng Formation unit 2 (A to C) are used for modeling.

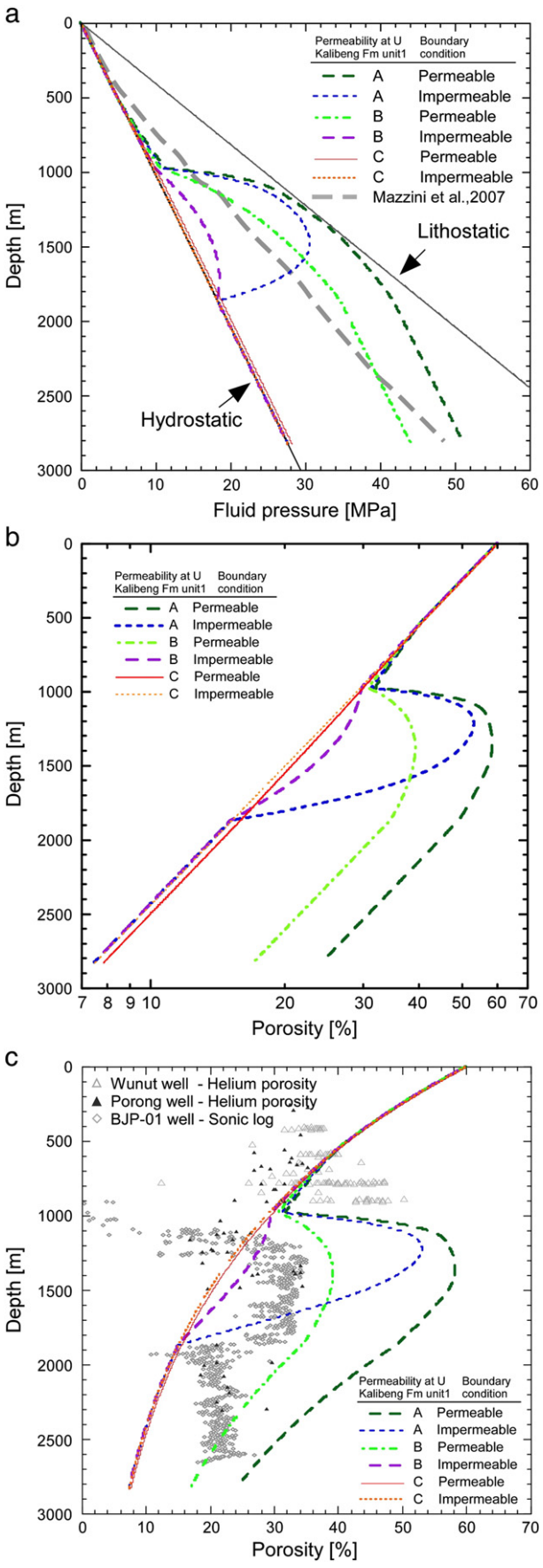

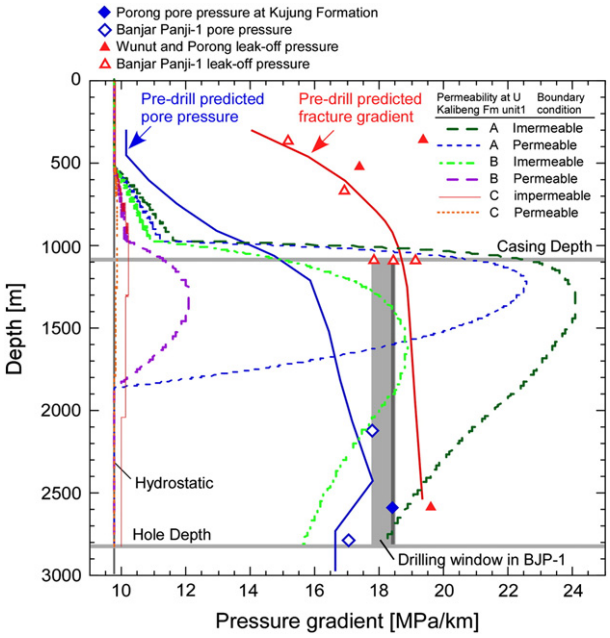

Fig. 9. Estimated fluid pressures for various conditions and reported fluid pressures and leak-off pressures in Banjar Panji-1 and the neighboring Porong and Wunut wells (compiled from Tingay et al., 2008; originally from Davies et al., 2007; Mazzini et al., 2007; and Sutriono, 2007) described by pressure gradients. We modeled four sets of boundary conditions at the base of the Kalibeng Formation and four permeabilities in the Upper Kalibeng 2 Formation (listed in Table 4).

fluidization (e.g., Maltman and Bolton, 2003). Liquefaction, which is the loss of friction between grain particles as a result of high sedimentation load and dilatancy, might have been caused at Lusi by the shear strain and the passage of seismic waves from regional earthquakes (Kano and Yanagidani, 2006), or possibly by a change in barometric pressure. Fluidization, which buoys muddy sediments, can be produced by the injection of liquid or gas into sediments at depth. Liquefaction commonly occurs after earthquakes in very shallow, sand-rich sediments, because it is much easier for fluid pressure to reach lithostatic pressure in shallow sedimentary layers than in deep layers. However, liquefaction of deep layers, such as those beneath mud volcanoes, is sometimes observed, though it is rare, and it is often related to the overpressure generation in layers of low permeability during basin evolution (Kopf, 2002). Therefore, the geological conditions at Lusi are similar to those known to form mud volcanoes.

Coseismically induced static changes in Coulomb failure stress and pore pressure as a result of the 2006 Yogyakarta earthquake have been well documented by Tingay et al. (2008) and Davies et al. (2008). The values they estimated for these were less than 1 kPa; these levels are likely too low to cause the mud volcano eruption by either remote (earthquake) triggering or by hydrofracturing. The dynamic stress (or pore pressure) change caused by ground motion and dilatational strain of seismic waves was also considered as a possible trigger by Tingay et al. (2008) and Davies et al. (2008). The amplitude of transient stress level estimated by Tingay et al. (2008) was 21 kPa, which is well below that necessary to cause remote triggering of fault reactivation, even though the level of transient change was greater than the static change. However, if high fluid

Fig. 8. Numerical modeling results for present-day (a) fluid pressure variations with depth and (b), (c) porosity variations with depth at the Lusi site. Numerical calculations were performed over the time range from 3.2 to 0 Ma. We modeled two sets of boundary conditions at the base of the Kalibeng Formation and four permeabilities in the Upper Kalibeng Formation unit 2 (listed in Table 4). Predicted pore pressures in (a) were modified from in situ measurements by Mazzini et al. (2007). Panel (b) was described by a log linear plot. Observed porosity data in (c) were modified from Lapindo Brantas Inc. (personal communication).

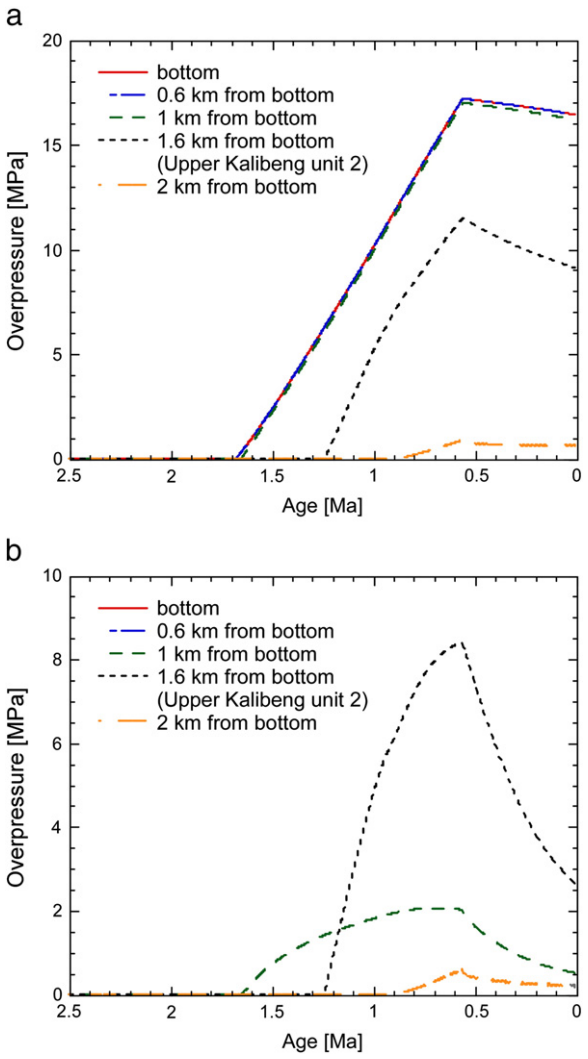

Fig. 10. Modeled evolution history of overpressure at various depths in the Banjar Panji-1 well assuming that the Upper Kalibeng 2 Formation is the cause of over pressure (case B in Table 4) with (a) a permeable boundary condition, and (b) an impermeable boundary condition. Calculations were over the time range from 3.2 Ma to the present.

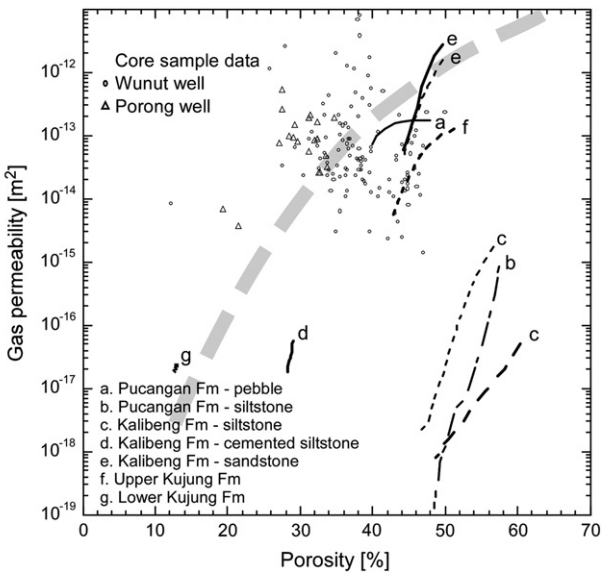

Fig. 11. Relationship between gas permeability and porosity for sedimentary rocks from the East Java Basin (this study) and core samples from Wunut well and Porong well (Lapindo Brantas Inc., personal communication). We collected Kalibeng Formation siltstone (curve c) and sandstone (e) at different locations, therefore two curves in each of the rocks are described.

pressure has been elevated at a lithostatic level at depth of the Lusi region, liquefaction potential will be increased by the reduction of rock strength, and thus the small amplitude of static or dynamic stress level will be enough to induce the liquefaction.

Temporal changes of dynamic stress lead to dynamic changes of permeability, and a reduction of permeability as a result of sudden consolidation of sediments will cause liquefaction as well. Our laboratory permeability data show weak dependence of permeability on effective pressure in the Kalibeng Formation at depth in the hydrostatic pressure condition (Fig. 7a), thus the permeability change by dynamic pore pressure change is not expected. On the other hand, the reduction of effective pressure due to overpressure generation can increase the pressure sensitivity of permeability (Fig. 5a), thus large changes of permeability that are likely to result from small change of dynamic stress by the earthquake might have induced liquefaction.

Additional influx of fluids into the Kalibeng Formation, which can assist fluidization, can be triggered by the fracture formations at depth during the ground motion of the Yogyakarta earthquake, or by the drilling of the Banjar Panji-1 well. Our modeling results show that fluid pressure in the Kalibeng Formation might have approached to formation pressure during the sedimentation history of the East Java Basin, therefore, many fractures might have been developed at depth during previous hydrofracturing events. These pre-existing fractures would have lower strengths than those of the undeformed rocks, and would be much more likely to be reactivated by the small perturbations related to the Yogyakarta earthquakes. Therefore the earthquake would have immediately formed new fractures as well as activated the pre-existing fractures that provided flow pathways through which large volumes of fluid could easily pass; otherwise, a tremendous release of muddy water would not have occurred. Even though the drilling induced fracturing seems to be much easier to form the flow pathways, our results support smaller perturbation of the earthquake will be enough to trigger for the fluidization.

Our data show that the Upper Kujung Formation is porous and permeable and that the Lower Kujung Formation has low porosity and is relatively impermeable with a small sensitivity of permeability to pressure change. This indicates that the Lower Kujung Formation has higher potential for overpressure generation than the Upper Kujung formation, although the latter acts as an aquifer, and is a likely source of fluids that would explain the long duration of the mud eruption. The limestone of the Kujung Formation is thought to be a source rock for hydrocarbons, and oil and natural gas occurrences are common in the Lusi region. Therefore, not only water but also a sudden inflow of gas and oil from the source rocks may have contributed to the mud eruption. Injection of gas and oil into the Kujung Formation would create a multiphase flow system and could change absolute permeability. Absorption of oil onto sediment grains can decrease water permeability, and this may enhance the generation of overpressure.

Davies et al. (2008) assumed a value of 1 for Skempton's coefficient, B, in their evaluation of pore pressure change as a result of earthquakes. However it was not certain for the assumption of the value of 1 in their model. Skempton's coefficient can be determined by the following equation (Wang, 2000) using our porosity data in laboratory test:

$$B = \left.\frac{\partial P}{\partial Pc}\right|_{\delta m_f = 0} = \frac{\beta_\Phi}{\beta_\Phi + \Phi\beta_f}, \tag{7}$$

where δm_f is the fluid mass content in porous material. Eq. (7) is a simplified equation that assumes that both unjacketed bulk compressibility and unjacketed pore compressibility are negligible. For the

Kalibeng Formation, *B* is in the range from 0.94 to 0.96 at depths of 1 to 2 km, which is consistent with the modeled parameter used by Davies et al. (2008).

7.2. Errors in our numerical modeling

Our basin model is very simple and neglects several factors that influence the generation of fluid pressure, for example, hydrocarbon generation, dehydration reactions, enhancement of flow by hydrofracturing, and additional influx of fluids from depth. If the volume of water expelled during dehydration and the amount of hydrocarbon generated by kerogen maturation (Luo and Vasseur, 1996) was high, the fluid pressures we determined in our modeling might be much below the true values. Additional fluid influx from depth greatly affects the pore pressure distribution (Tanikawa et al., 2008). The Kujung Formation might have been a source for a considerable influx of water or hydrocarbons because the dominant carbonates of this formation are thought to provide both a source and reservoir for hydrocarbons. There is an andesitic volcanic arc close to and south of Lusi; consequently, there is active volcanism in the area. Therefore, the heat flux and geothermal gradient at Lusi is high, which would enhance the influx of water or hydrocarbons from depth as a result of heat-related chemical reactions. Hydrofracturing is caused when pore pressure approaches minimum principal stress, and permeability will be enhanced by the fracturing. However, the great uncertainty in the modeling is the assumed change in permeability during hydrofracturing. The model also limited in one-dimensional analysis, though two dimensional flow analysis is more appropriate.

We found large differences between water and gas permeabilities. A higher permeability of rocks to gas than to water is generally explained by the Klinkenberg effect. That is, the flow rate of gas is increased by “slip flow”, which is enhanced gas flow at the pore wall (grain) surface caused by collisions between gas molecules and the solid pore walls (Wu et al., 1998). However, the water permeability in the East Java Basin is much lower than the gas permeability in the same formation and it is difficult to explain by the Klinkenberg effect alone. The sedimentary rocks of the East Java Basin are relatively young and soft, and the gap between water and gas permeability is larger in the siltstones than in the sandstones and limestones. Siltstones in the Upper Kalibeng Formation contain considerable amounts of swelling clays (smectite); therefore, adsorption-induced swelling of the clay matrix reduces available pore space and flow paths, and thus decreases permeability in these rocks (Zhang et al., 2008). In addition, the strength of rocks that contain clay minerals is decreased by water saturation (Ibanez and Kronenberg, 1993; Morrow et al., 2000). The weakening of these rocks by water saturation happens because the sheet-structured minerals have charged surfaces that adsorb water easily, and this water reduces the frictional strength between particles. Therefore, strength reduction induced by water adsorption can enhance consolidation and therefore decrease permeability.

As we were unable to collect core samples from the Banjar Panji-1 borehole, we used surface-quarried samples to estimate in situ transport properties by using ex situ laboratory tests. This may have introduced errors in our modeling because of the unloading of burial pressures for outcrop samples and the effects of weathering. These processes can produce both microcracks and macrocracks, which reduce the pressure sensitivity of permeability and increase permeability in general (Morrow and Lockner, 1994). Moreover, permeability measured in situ is commonly higher than that determined in the laboratory because of enhanced flow in mesoscopic- and macroscopic-scale fractures in situ (Brace, 1980). The gas permeability we measured in the Pucangan Formation outcrop samples was reasonably consistent with that derived from core samples (Fig. 7), although there was a large difference between our gas permeability measurements in the Upper Kalibeng Formation and the permeabilities measured in core samples. Porosity of surface-derived samples we measured was larger than porosity of samples from boreholes and the porosity from sonic-log data (Fig. 2). However, pressure sensitivity of porosity in outcrop samples is similar to borehole data, which shows that both specific storage and pressure sensitivity to specific storage measured using outcrop samples are similar to those from borehole data (Fig. 7c). The relative higher porosity in outcrop samples are explained by the surface weathering that produces micro cracking and micro-pores, though the relative lower permeability cannot be explained by the same process. If in situ permeability is higher than our laboratory data, overpressure generation becomes smaller in our numerical modeling. In situ stress state shows anisotropy in common, and the difference between minimum and maximum principal stress may be several ten MPa at depth (Zoback and Healy, 1992). Therefore, permeability and porosity measured in laboratory test under hydrostatic loading condition might be different from in situ data under triaxial stress state.

8. Conclusions

Our laboratory results show that permeability in the Kalibeng Formation, which is considered to be the mud source for Lusi, is very low, ranging from 10^{-19} to 10^{-20} m^2. The Upper Kujung Formation is porous and permeable, but the Lower Kujung Formation is much less so. Our basin analysis in the Lusi area showed that overpressure was generated and maintained within the Kalibeng Formation, mainly because of the combined effects of a rapid sedimentation rate and the low permeability of the Kalibeng Formation. The characteristic of fluid pressure distribution is similar to that estimated from drilling data. The reduction of rock strength as a result of long-term high fluid pressure might have influenced the mud eruption, because low rock strength favors the generation of liquefaction and hydrofracturing at low levels of dynamic pore pressure fluctuation such as those that might have been triggered by the Yogyakarta earthquake. We believe that a rapid and massive influx of gas and liquid from the Kujung Formation flowing through pre-existing pathways formed by hydrofracturing during the basin evolution explains the continuous mud eruption at Lusi. The regional long-term evolution of fluid pressures in thick mud layers plays a great part in the formation of mud volcanoes on the island of Java in Indonesia.

Acknowledgements

We are very grateful to Nurrochmat Sawolo and Dr. Van Williams for their comments on this manuscript. We also thank Hade B. Maulin for his support during our field trip to East Java. We are very grateful to Lapindo Brantas Inc. for providing the well data we used in this study. Thanks also to an anonymous reviewer for comments on the manuscript.

References

Athy, L.F., 1930. Density, porosity, and compaction of sedimentary rocks. AAPG Bull. 14, 1–22.
Bernabe, Y., 1987. A wide range permeameter for use in rock physics. Int. J. Mech. Min. Sci. Geomech. Abstr. 24 (5), 309–315.
Bethke, C.M., Corbet, F., 1988. Linear and nonlinear solutions for one-dimensional compaction flow in sedimentary basins. Water Resour. Res. 24, 461–467.
Birch, F., 1966. Compressibility, elastic constants. In: Clark, S.P. (Ed.), Handbook of Physical Constants: Geol. Soc. Am. Mem., 97, pp. 97–173.
Brace, W.F., 1980. Permeability of crystalline and argillaceous rocks. Int. J. Mech. Min. Sci. Geomech. Abstr. 17, 241–251. doi:10.1016/0148-9062(80)90807-4.
Bredehoeft, J.D., Hanshaw, B.B., 1968. On the maintenance of anomalous fluid pressures: I. Thick sedimentary sequences. Geol. Soc. Am. Bull. 79 (9), 1097–1106.
Davies, R.J., Swarbrick, R.E., Evans, R.J., Huuse, M., 2007. Birth of a mud volcano: East Java, 29 May 2006. GSA Today 17, 4–9.
Davies, R.J., Brumm, M., Manga, M., Rubiandini, R., Swarbrick, R., Tingay, M., 2008. The East Java mud volcano (2006 to present): an earthquake or drilling trigger? Earth Planet. Sci. Lett. 272, 627–638.
Fontaine, F.J., Rabinowicz, M., Boulègue, J., 2001. Permeability changes due to mineral diagenesis in fractured crust: implications for hydrothermal circulation at mid-

ocean ridges. Earth Planet. Sci. Lett. 184 (2), 407–425. doi:10.1016/S0012-821X(00)00332-0.
Gibson, R.E., 1958. The progress of consolidation in a clay layer increasing in thickness with time. Geotechnique 8, 171–182.
Hirono, T., Takahashi, M., Nakashima, S., 2003. In-situ visualization of fluid flow image within deformed rock by X-ray CT. Eng. Geol. 70, 37–46.
Ibanez, W.D., Kronenberg, A.K., 1993. Experimental deformation of shale: mechanical properties and microstructural indicators of mechanisms. Int. J. Mech. Min. Sci. Geomech. Abstr. 30, 723–734.
Kano, Y., Yanagidani, T., 2006. Broadband hydroseismograms observed by closed borehole wells in the Kamioka mine, central Japan: response of pore pressure to seismic waves from 0.05 to 2 Hz. J. Geophys. Res. 111, B03410. doi:10.1029/2005JB003656.
Kopf, A.J., 2002. Significance of mud volcanism. Rev. Geophys. 40. doi:10.1029/2000RG000093.
Kusumastuti, A., Van Rensbergen, P., Warren, J.K., 2002. Seismic sequence analysis and reservoir potential of drowned Miocene carbonate platforms in the Madura Strait, East Java, Indonesia. AAPG Bull. 86, 213–232.
Luo, X., Vasseur, G., 1992. Contribution of compaction and aquathermal pressuring to geopressure and the influence of environmental conditions. AAPG Bull. 76, 1550–1559.
Luo, X., Vasseur, G., 1996. Geopressuring mechanism of organic matter cracking: numerical modeling. AAPG Bull. 80, 856–874.
Magara, K., 1968. Compaction and migration of fluids in Miocene mudstone, Nagaoka Plain, Japan. AAPG Bull. 52, 2466–2501.
Maltman, A.J., Bolton, A., 2003. How sediments become mobilized. In: Van Rensbergen, P., Hillis, R.R., Maltman, A.J., Morley, C.K. (Eds.), Subsurface Sediment Mobilization, 216. Geological Society Special Publications, pp. 9–20.
Mazzini, A., Svensen, H., Akhmanov, G.G., Aloisi, G., Planke, S., Malthe-Sørenssen, A., Istadi, B., 2007. Triggering and dynamic evolution of the LUSI mud volcano, Indonesia. Earth Planet. Sci. Lett. 261, 375–388.
Morrow, C., Lockner, D., 1994. Permeability differences between surface-derived and deep drillhole core samples. Geophys. Res. Lett. 21 (19), 2151–2154.
Morrow, C., Bo-Chong, Z., Byerlee, J., 1986. Effective pressure law for permeability of westerly granite under cyclic loading. J. Geophys. Res. 91 (B3), 3870–3876.
Morrow, C.A., Moore, D.E., Lockner, D.A., 2000. The effect of mineral bond strength and adsorbed water on fault gouge frictional strength. Geophys. Res. Lett. 27, 815–818.
Osborn, M.J., Swarbrick, R.E., 1997. Mechanisms for generating overpressure in sedimentary basins: a reevaluation. AAPG Bull. 81 (6), 1023–1041.
Plumlee, G.S., Casadevall, T.J., Wibowo, H.T., Rosenbauer, R.J., Johnson, C.A., Breit, G.N., Lowers, H.A., Wolf, R.E., Hageman, P.L., Goldstein, H., Anthony, M.W., Berry, C.J., Fey, D.L., Meeker, G.P., Morman, S.A., 2008. Preliminary analytical results for a mud sample collected from the LUSI mud volcano, Sidoarjo, East Java, Indonesia. USGS Open-File Report, p. 1019.
Pudasaini, S.P., Hutter, K., 2007. Avalanche Dynamics : Dynamics of Rapid Flows of Dense Granular Avalanches. Springer-Verlag GmbH, Berlin Heidelberg. 626 pp.
Raiga-Clemenceau, J., Martin, J.P., Nicoletis, S., 1988. The concept of acoustic formation factor for more accurate porosity determination from sonic transit time data. Log Analyst 29, 54–60.
Scheidegger, A.E., 1974. The Physics of Flow Through Porous Media, 3rd Edition. University of Toronto Press, Toronto.
Schiller, D.M., Seubert, B.W., Musliki, S., Abdullah, M., 1994. The reservoir potential of Globigerinid sands in Indonesia. Proc. 23rd Annual Convention Proceedings of Indonesian Petroleum Association, 1. 189ff.
Sutriono, E., 2007. Pemboran Sumur Eksplorasi Banjarpanji-1. Proceedings of the International Geological Workshop on Sidoarjo Mud Volcano, Jakarta, February 20–21, 2007. Indonesia Agency for the Assessment and Application of Technology, Jakarta.
Tanikawa, W., Shimamoto, T., 2009. Comparison of Klinkenberg-corrected gas permeability and water permeability in sedimentary rocks. Int. J. Mech. Min. Sci. 46, 229–238.
Tanikawa, W., Shimamoto, T., Wey, S.-K., Lin, C.-W., Lai, W.-C., 2008. Stratigraphic variation of transport properties and overpressure development in the Western Foothills, Taiwan. J. Geophys. Res. 113. doi:10.1029/2008JB005647.
Tingay, M., Heidbach, O., Davies, R., Swarbrick, R., 2008. Triggering of the Lusi mud eruption: earthquake versus drilling initiation. Geology 36, 639–642.
Wang, H.F., 2000. Theory of linear poroelasticity: with applications to geomechanics and hydrogeology. Princeton Series in Geophysics. Princeton University Press, Princeton. 287 pp.
Wangen, M., 2001. A quantitative comparison of some mechanisms generating overpressure in sedimentary basins. Tectonophysics 334, 211–234.
Wibberley, C.A.J., Shimamoto, T., 2005. Earthquake slip weakening and asperities explained by thermal pressurization. Nature 436, 689–692.
Willumsen, P., Schiller, D.M., 1994. High quality volcaniclastic sandstone reservoirs in East Java, Indonesia. IPA, 23rd Annual Convention, vol. I, pp. 101–111.
Wu, B., Tan, C. P., Aoki, T., 1997. Specially designed techniques for conducting consolidated undrained triaxial tests on low permeability shales. *Int. J. Mech. Min. Sci.*, 34:3–4, Paper No. 336.
Wu, Y.S., Pruess, K., Persoff, P., 1998. Gas flow in porous media with Klinkenberg's effect. Transp. Porous Media 32, 117–137.
Zhang, H., Liu, J. Elsworth, D., 2008. How sorption-induced matrix deformation affects gas flow in coal seams: a new FE model. *Int. J. Mech. Min. Sci.*, 45, 8, 1226–1236.
Zoback, M.D., Byerlee, J.D., 1975. The effect of microcrack dilatancy on the permeability of Westerly Granite. J. Gephys. Res. 80, 752–755.
Zoback, M.D., Healy, J.H., 1992. In situ stress measurements to 3.5 km depth in the Cajon Pass scientific research borehole: implications for the mechanics of crustal faulting. J . Geophys. Res. 97 (B4), 5039–5057.